Terahertz Quantum Cascade Lasers and Electronics

Academic and Research Staff
Professor Qing Hu

Postdoctoral Associates
Benjamin S. Williams

Graduate Students
Hans Callebaut, Steve Kohen, Kostas Konistis, Sushil Kumar, Juan Montoya

Introduction

Millimeter-wave and THz frequencies (f = 0.1-10 THz) remain one of the most underdeveloped frequency ranges, even though the potential applications in remote sensing and imaging, spectroscopy, and communications are great. This is because the millimeter-wave and THz frequency range falls between two other frequency ranges in which conventional semiconductor devices are usually operated. One is the microwave frequency range, and the other is the near-infrared and optical frequency range. Semiconductor devices which utilize the classical diffusive transport of electrons, such as diodes and transistors, have a high frequency limit. This limit is set by the transient time and parasitic RC time constants. Currently, electron mobility and the smallest feature size which can be fabricated by lithography limit the frequency range to below several hundred GHz. Semiconductor devices based on quantum mechanical interband transitions, however, are limited to frequencies higher than those corresponding to the semiconductor energy gap, which is higher than 10 THz for most bulk semiconductors. Therefore, a large gap exists from 1 to 10 THz in which very few devices are available.

Semiconductor quantum-effect devices (which can be loosely termed "artificial atoms"), including both vertically grown quantum-well structures and laterally confined mesoscopic devices, are human-made quantum mechanical systems in which the energy levels can be chosen by changing the sizes of the devices. Typically, the frequency corresponding to the intersubband transitions is in the millimeter-wave range ($\Delta E \sim$ 1-4 meV) for the lateral quantum-effective devices, and THz to infrared for the vertical quantum wells. It is therefore appealing to develop ultrahigh-frequency devices, such as THz lasers utilizing the intersubband transitions in these devices.

In our group, we are systematically investigating physical and engineering issues that are relevant to devices operating from millimeter-wave to THz frequencies. Specifically, we are working on THz quantum cascade lasers based on intersubband transitions in quantum wells, ultrahigh-frequency heterostructure bipolar transistors based on phonon-enhanced forward diffusion, and on-chip terahertz spectrometers using ultrafast photoconductive switches.

Terahertz quantum cascade lasers

Sponsors
National Science Foundation
Grant ECS-0217782
NASA
Grant NNG04GC11G
AFOSR
Grant F49620-00-1-0331
DOD NGSEG fellowship

Project Staff
Ben Williams, Hans Callebaut, Sushil Kumar, Steve Kohen, and Qing Hu, in collaboration with Dr. John Reno at Sandia National Lab.

Semiconductor quantum wells are human-made quantum mechanical systems in which the energy levels can be designed and engineered to be of any value. Consequently, unipolar lasers based on intersubband transitions (electrons that make lasing transitions between subband levels within the conduction band) were proposed for long-wavelength sources as early as the 1970s. However, because of the great challenge in epitaxial material growth and the unfavorable fast nonradiative relaxation rate, unipolar intersubband-transition lasers (also called quantum-cascade lasers) at mid-infrared wavelengths were developed only recently at Bell Laboratories. This achievement paved the way for development of coherent laser sources at customized frequencies ranging from THz to near-infrared. However, compared to the infrared QCLs, THz QCLs at much longer wavelengths face unique challenging issues. First, the energy levels corresponding to THz frequencies (1 THz = 4 meV) are quite narrow, so it is very challenging to design quantum well structures for selective injection to the upper level and selective depopulate electrons from the lower level. The requirements for fabrication of such quantum-well structures with adequate accuracies are also demanding. Because of the narrow separation between subband levels, heating and electron-electron scattering will have a much greater effect. Also, the small energy scales of THz photons make the detection and analysis of spontaneous emission (a crucial step toward developing lasers) quite difficult. Second, mode confinement, which is essential for any laser oscillation, is difficult at longer wavelengths. Conventional dielectric-waveguide confinement is not applicable because the evanescent field penetration, which is proportional to the wavelength and is on the order of several tens of microns, is much greater than the active gain medium of several microns. Recently (November 2002), we made a breakthrough in developing quantum-cascade lasers at 3.4 THz (corresponding to 87 μm wavelength). Since then, we have made rapid progress in developing many lasers with record performance, including but not limited to the highest pulsed operating temperature of 137 K, highest CW operating temperature of 93 K, and the longest wavelength of 141 μm (corresponding to 2.1 THz). Key results are summarized in the following sections.

THz quantum cascade lasers based on resonant phonon scattering for depopulation

The direct use of LO-phonon scattering for depopulation of the lower state offers several distinctive advantages. First, when a collector state is separated from the lower state by at least the phonon energy $\hbar\omega_{LO}$, depopulation can be extremely fast, and it does not depend much on temperature or the electron distribution. Second, the large energy separation provides intrinsic protection against thermal backfilling of the lower radiative state. Both properties are important in allowing higher temperature operation of lasers at longer wavelengths.

The present design combines advantages of our two previously investigated THz emitters. As shown in Fig. 1, the radiative transition between levels 5 and 4 is spatially vertical, yielding a large oscillator strength. The depopulation is highly selective, as only the lower level 4 is at resonance with a level 3 in the adjacent well, where fast LO-phonon scattering takes place. The

four-well structure inside the dashed box is one module of the structure, and 175 such modules are connected in series to form the quantum cascade laser.

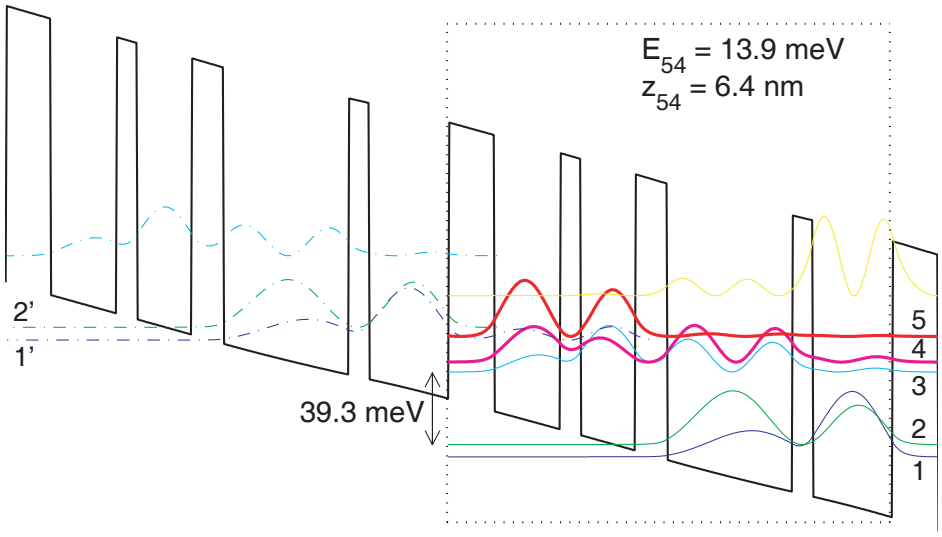

Figure 1. Conduction band profile calculated using a self-consistent Schrödinger and Poisson solver (80% conduction band offset) biased at 64 mV/module. Beginning with the injector barrier, the layer thickness in Å are 54/78/24/64/38/148/24/94. The 148-Å well is doped with Si at $1.9\times10^{16}/cm^3$, yielding a sheet density of $2.8\times10^{10}/cm^2$.

Mode confinement in this laser device was achieved using a surface plasmon layer grown under the active region. The schematic of the device structure and the calculated mode profile and waveguide loss are shown in Fig. 2. The calculated waveguide loss of 7.1 cm^{-1} and mode confinement factor $\Gamma \approx 29\%$ are quite favorable compared to the calculated gain of our laser device.

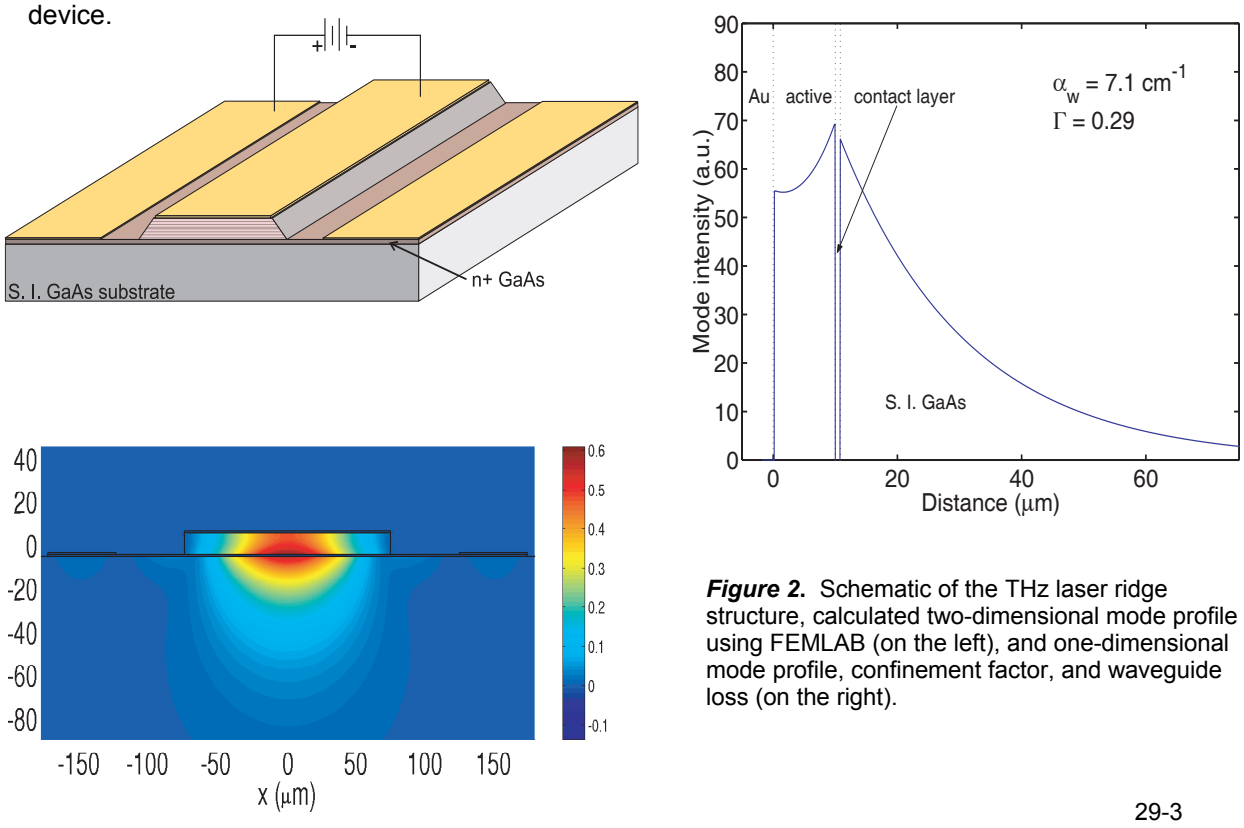

Figure 2. Schematic of the THz laser ridge structure, calculated two-dimensional mode profile using FEMLAB (on the left), and one-dimensional mode profile, confinement factor, and waveguide loss (on the right).

Lasing at 3.38 THz (λ = 88.6 μm) was obtained in this device at a threshold current density of ~800 A/cm^2 at 5 K from a 200-μm wide and 2.6-mm long laser structure. A typical emission spectrum above threshold is shown in Fig. 3(a). The emission frequency corresponds to a photon energy of 14.0 meV, close to the calculated value of 13.9 meV. For much of the bias range, the emission is predominantly single mode, although the spectrum shifts toward a higher mode with increasing bias, due to the Stark shift. Pulsed lasing operation is observed up to 87 K with a power level (measured using a calibrated thermopile detector, ScienTech Model #360203) of 13 mW at 5 K, and ~4 mW even at liquid-nitrogen temperature of 78 K, as shown in Fig. 3(b). In fact, the spectrum shown in Fig. 3(a) was taken with the laser device cooled by liquid nitrogen and using the internal room-temperature pyroelectric detector of a Nicolet FTIR in the fast-scan mode. Measured from a shorter and narrower bar structure (150-μm by 1-mm), Fig. 3(c) displays the voltage versus current, as well as several *P-I* curves taken for pulses of increasing width. Even at a high 50% duty cycle, the laser still produces ~2 mW of peak power, indicating its robustness.

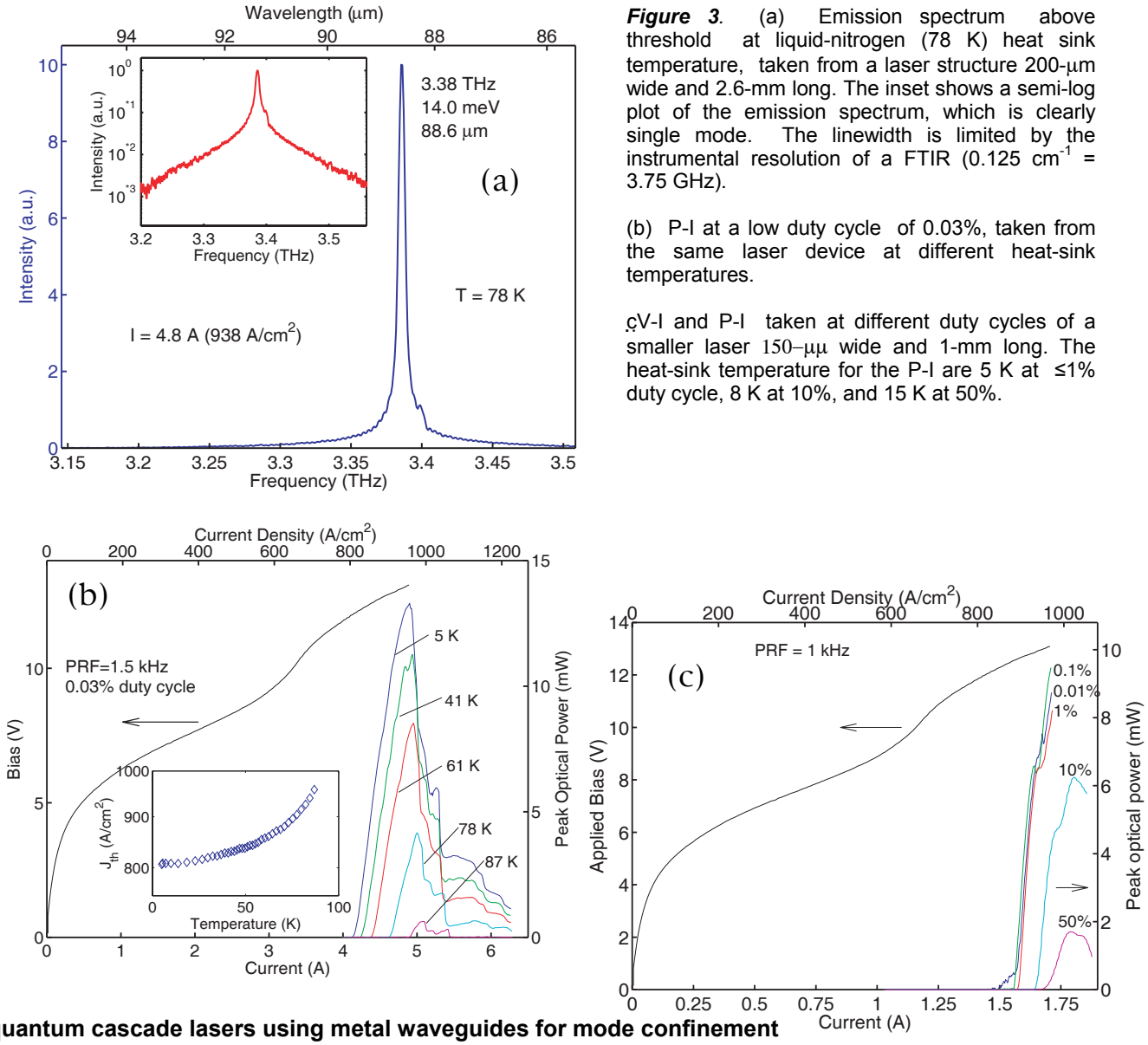

Figure 3. (a) Emission spectrum above threshold at liquid-nitrogen (78 K) heat sink temperature, taken from a laser structure 200-μm wide and 2.6-mm long. The inset shows a semi-log plot of the emission spectrum, which is clearly single mode. The linewidth is limited by the instrumental resolution of a FTIR (0.125 cm^{-1} = 3.75 GHz).

(b) P-I at a low duty cycle of 0.03%, taken from the same laser device at different heat-sink temperatures.

çV-I and P-I taken at different duty cycles of a smaller laser 150–μμ wide and 1-mm long. The heat-sink temperature for the P-I are 5 K at ≤1% duty cycle, 8 K at 10%, and 15 K at 50%.

THz quantum cascade lasers using metal waveguides for mode confinement

After our initial success in the development of 3.4-THz quantum cascade laser, one of the improvements made was the mode confinement. As shown in Fig. 2, the mode confinement using surface plasmon layer yields a relatively low mode confinement factor of $\Gamma \approx 0.29$. This mode confinement is sufficient for lasing at 3.4 THz. However, as we are developing even longer wavelength quantum cascade lasers, the mode confinement will become much worse or even unconfined at frequencies lower than 2 THz for the carrier concentration in our laser structures. An alternative method for mode confinement is to use metal waveguides. As shown in Fig. 4, the mode is now tightly confined between the top and bottom metal contacts, yielding a confinement factor close to 100%. Fig. 4 also shows the process of wafer bonding and selective etching to fabricate such a metal waveguide structure.

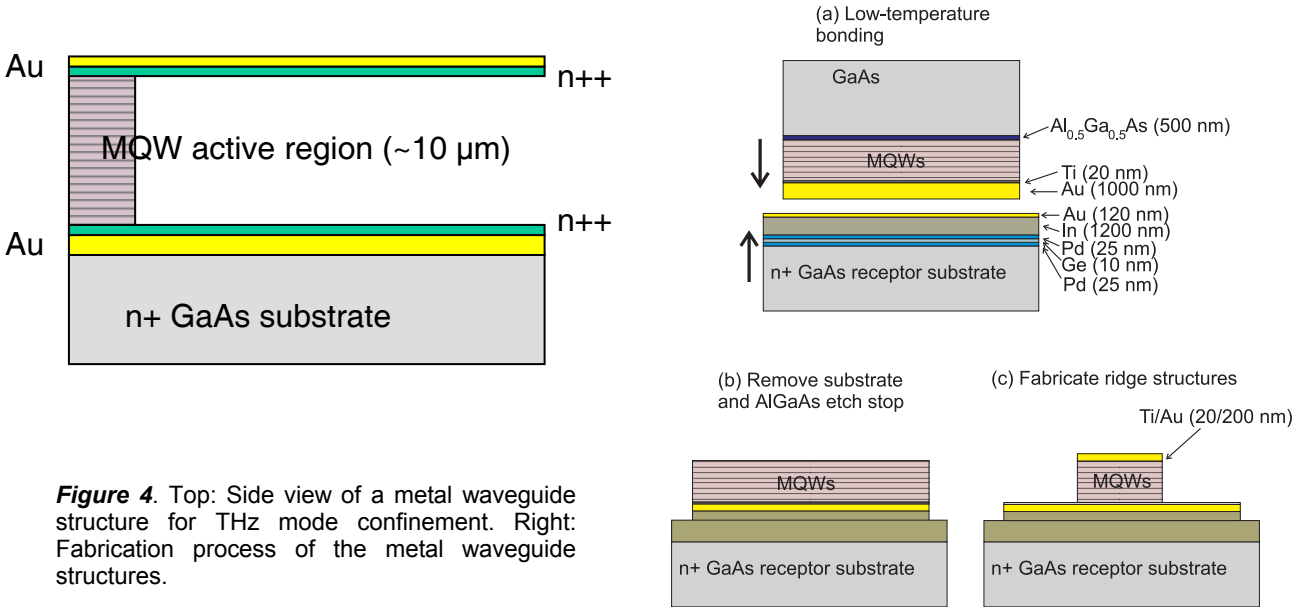

Figure 4. Top: Side view of a metal waveguide structure for THz mode confinement. Right: Fabrication process of the metal waveguide structures.

Using a combination of the metal-metal waveguides and improved gain medium, we have developed THz QCLs with many record performance in the last year. Some of the highlights of these achievements are summarized in Fig. 5, including the highest operating temperature of 137 K in the pulsed mode, 93 K in CW mode, and the longest wavelength (141 μm, corresponding to 2.1 THz) QCL to date.

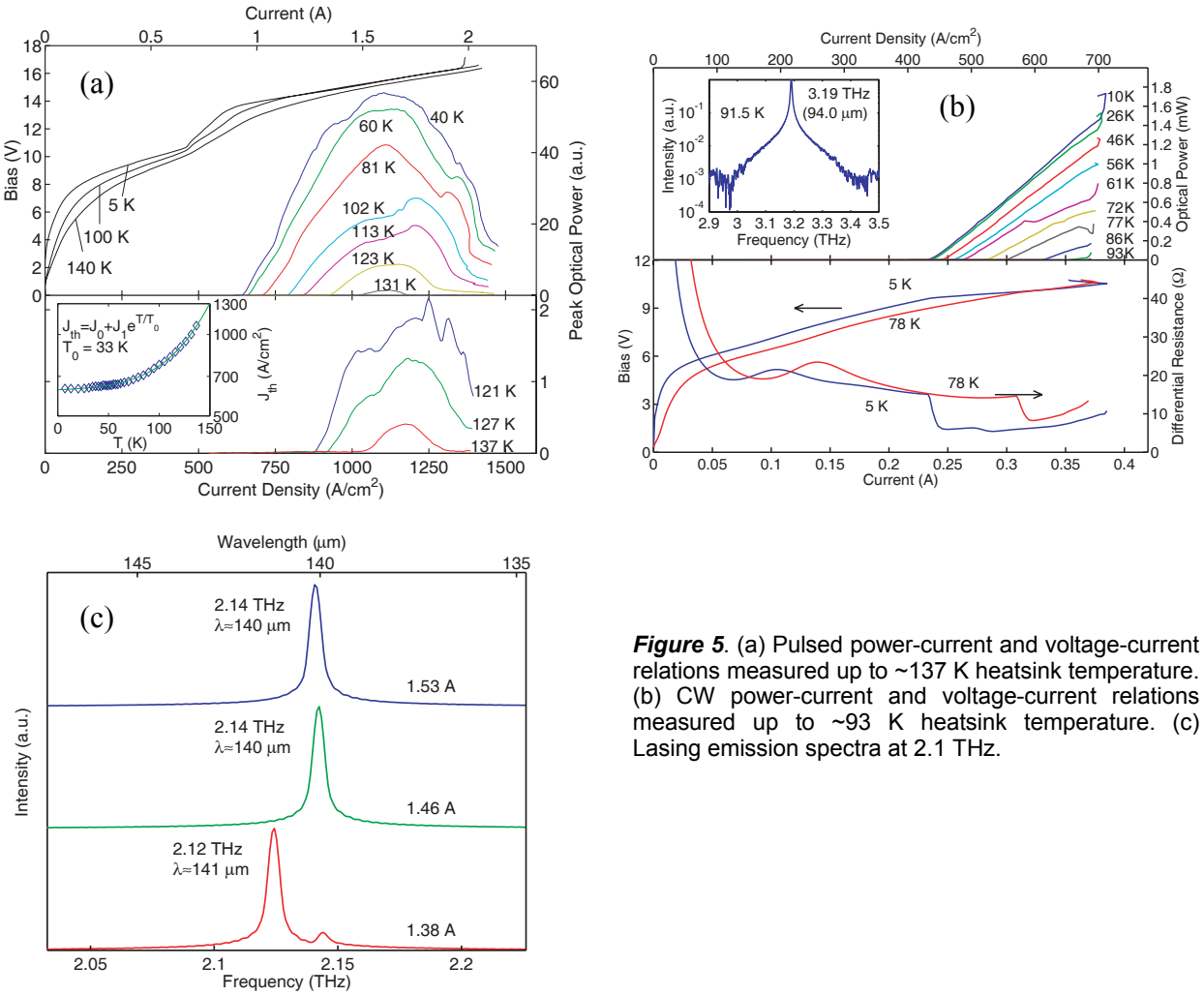

Figure 5. (a) Pulsed power-current and voltage-current relations measured up to ~137 K heatsink temperature. (b) CW power-current and voltage-current relations measured up to ~93 K heatsink temperature. (c) Lasing emission spectra at 2.1 THz.

Analysis of transport properties of THz quantum cascade lasers

Even though mid-infrared and THz quantum cascade lasers operate on the same principle, that is, intersubband transition in semiconductor heterostructures, they show a qualitative difference in the dynamics of electron transport. For mid-infrared QCLs, the subband separations exceed the LO-phonon energy $\hbar\omega_{LO}$ and electron transport is dominated by LO-phonon scattering. For THz QCLs, many subband separations are smaller than $\hbar\omega_{LO}$, only the high-energy tail of a hot electron distribution is subject to the LO-phonon scattering, which results in a significantly higher temperature sensitivity for the electron transport and a far greater importance of electron-electron (e-e) scattering. The long delay in the development of THz QCLs is testimony to the difficulty of achieving population inversion involving these complicated transport mechanisms. It is thus important to quantitatively model these transport processes to extend the operation of THz QCLs to broader frequency ranges and higher temperatures.

Our transport analysis is based on Monte Carlo (MC) simulations, which have been used to analyze and design mid-infrared and THz QCLs. Compared to conventional rate-equation analysis, the MC method is especially useful for THz QCLs, as it does not rely on a specific model for carrier distributions and can easily handle temperature- and density-dependent scattering times. Fig. 6 illustrates the flow chart of our Monte Carlo simulation scheme. It follows

a conventional scheme for an ensemble of particles, in our case 10^4 particles, with a focus on e-e and e-phonon interactions involving the electrons in one module of the device under study. An electron that scatters out of a module is reinjected with identical in-plane *k*-vector into a subband equivalent to its destination subband, in accordance with the spatial periodicity of QCLs.

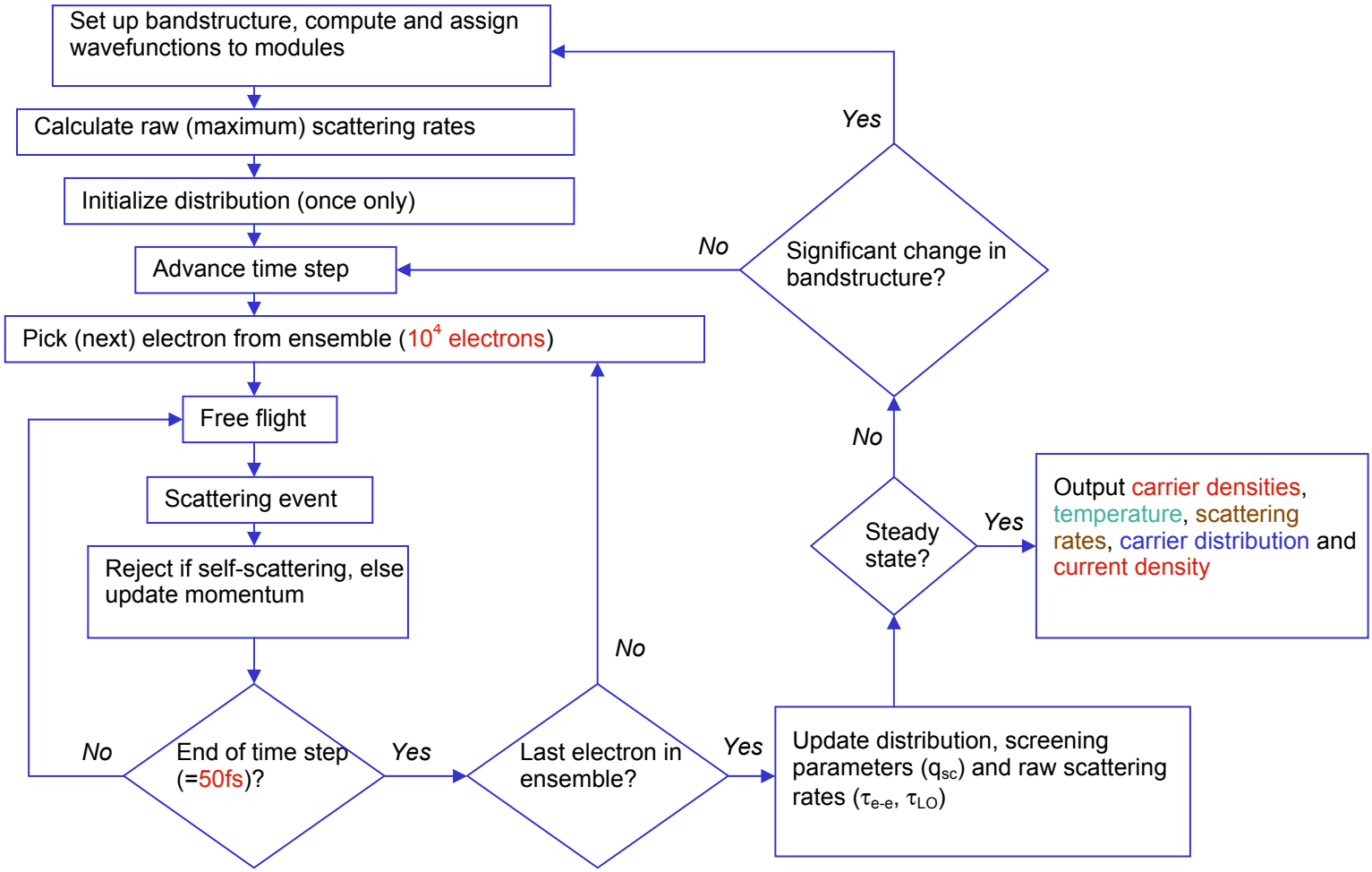

Figure 6. Flow chart of our ensemble Monte Carlo simulation scheme.

The results of the Monte Carlo simulations, focused on the 3.4-THz laser structure shown in Fig. 1, are summarized in Fig. 7. All simulations assumed a lattice temperature of 25 K, corresponding to a 10 K heat sink temperature. In Fig. 8(a), the calculated I-V relation qualitatively resembles that of measured one, with the calculated peak current density is noticeable lower. This discrepancy suggests the scattering processes in the MC simulations are slower than in actual devices. The slower scattering processes yielded a higher calculated peak gain than inferred from experiments, as shown in Fig. 7(d). The two horizontal lines are calculated total cavity losses with one facet Au coated and without any facet coating. Our device lased only with one facet coating, thus the two lines define the range of material gain in our laser device. The qualitative agreement between the MC and experimental results indicate the usefulness of MC simulation as a design tool. The discrepancy requires further investigation of all important scattering channels.

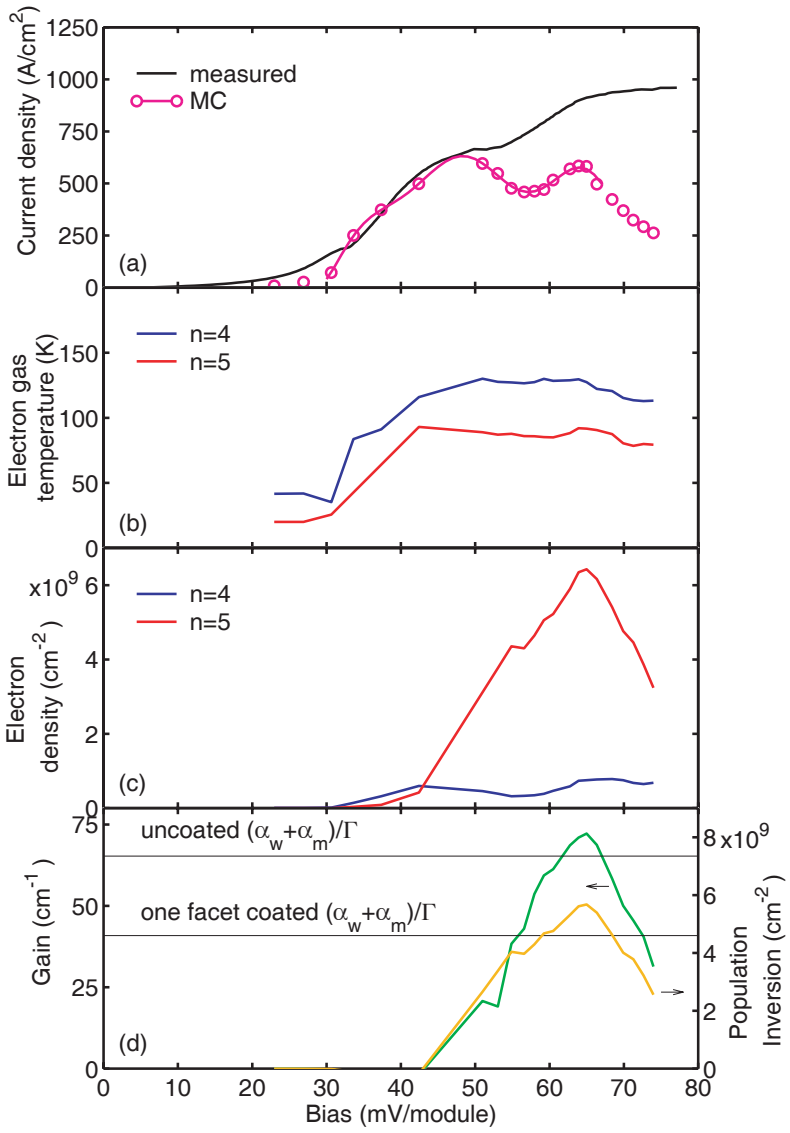

Figure 7. Key results of the MC simulation for a lattice temperature of 25 K.

(a) Current density for a range of bias voltage. The injection anticrossing occurs at 65 mV/module.

(b) Electron temperature for the subbands involved in the radiative transition, $n = 4$ and $n = 5$.
(c) The population density in $n = 4$ and $n = 5$.

(d) Material gain and population inversion for different biases.

AlGaAs/GaAs HBT with enhanced forward diffusion

Sponsors
AFOSR
Grant F49620-00-1-0331

Project Staff
Kostas Konistis and Qing Hu, in collaboration with Prof. M. Melloch at Purdue University, and Prof. C. G. Fonstad.

One of the key limits of high-frequency operation of bipolar transistors is the base transient time, which is proportional to the square of the base width when the base transport is dominated by diffusion. Consequently, high-frequency bipolar transistors tend to use thin bases (<100 nm) that results in a short base transient time and a high cut-off frequency f_T. However, for high frequency operations, it is not the current gain that matters most. Rather, it is the unilateral power gain that determines the operating frequency of any three-terminal devices. The frequency f_{max}, at which the power gain is unity, is determined by both f_T and *RC* time constant. Because of the peculiar geometry of bipolar transistors, the electrical contact to the base is always made from the side. Thus, a thin base, which is important to yield a high f_T, will inevitably result in a high sheet resistance and a lowering of f_{max}. It is this difficult trade-off between f_T and f_{max} that lead Prof. S. Luryi and his co-workers to propose a novel heterostructure bipolar transistor, whose band diagram is shown in Fig. 8.

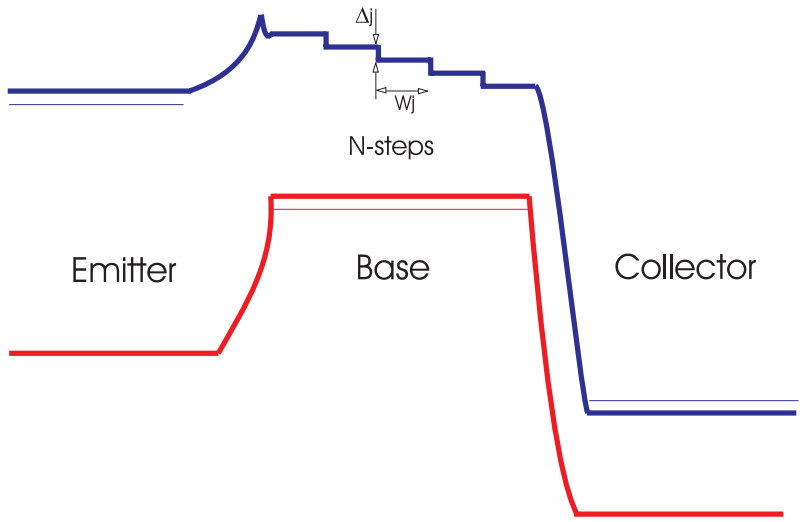

Figure 8. Energy band diagram of an HBT with stepwise base. The energy drop Δ at each step is slightly greater than the LO-phonon energy (36 meV) in GaAs. Thus, electrons encounter very fast LO-phonon emission scattering (with a time ~0.1 ps) when they go over the edge of a step. Consequently, backward diffusion is significantly reduced and forward diffusion is enhanced.

The main feature of this novel HBT is that its base is graded like a staircase. The height of each step Δ is slightly greater than the LO-phonon energy in GaAs (36 meV). Thus, electrons will encounter very fast LO-phonon emission scattering (with a time ~0.1 ps) when they go over the edge of a step. Consequently, backward diffusion is significantly reduced. In a way, the edge of each step resembles and performs a similar function as the base-collector interface: any injected excess minority carrier will be quickly swept down the energy potential. As a result, each step acts like a minibase, as far as the diffusion transport is concerned. The resulting minority carrier concentration assumes a nearly periodic distribution, provided that the energy drop is greater than the sum of LO-phonon and thermal energy to ensure a fast scattering and prohibit backward

diffusion. The total base transient time is therefore approximately N times the transient time of each step, whose width can be as narrow as 30 nm, yielding a high f_T. On the other hand, all the N steps are connected in parallel for the base contact, reducing the base resistance by an approximate factor of N. The combination of a thin effective base and small base resistance will yield a high f_{max}.

One interesting result of our analysis is the existence of resonances of the unilateral power gain. Their physical mechanism is closely linked with the current-phase delay. A base structure introduces both phase delay and magnitude attenuation of current. As the frequency of operation increases, the phase delay increases and at a certain frequency the voltage and current acquire opposite phases, which will yield a resonance if the amplitude attenuation is not too overwhelming. A short base offers small phase delay and resonance occurs at high frequencies where the magnitude attenuation is strong. On the other hand, a long base may provide a large phase delay but the heavy attenuation at low frequencies smoothes out the unilateral gain peaks. For a multi-step base, the total phase delay is the sum of each step, while the total attenuation is the product of each step, enhancing the possibilities of achieving resonance. As can be seen in Fig. 9, the unilateral power gain exhibits multiple resonances beyond typical cut-off frequencies (f_T) for multiple-step HBTs. These resonance can be achieved above 100 GHz, which is promising for the development of high-frequency amplifiers and fundamental oscillators.

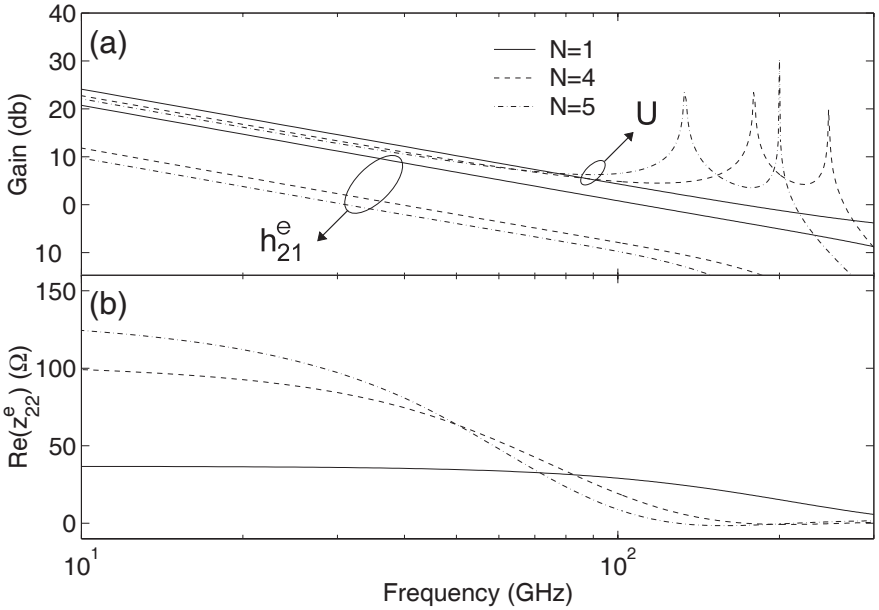

Figure 9. (a) Unilateral power gain magnitude, current gain magnitude, and (b) output resistance for X_{step} = 500Å, Δ = 1.2 $\hbar\omega_{LO}$. As the number of steps increases (N = 1,4,5), *U* extends in frequency by means of resonance.

We have developed an elaborated process to fabricate very high-frequency HBTs using airbridges for electrode isolation. Fig. 10 shows the schematic of the device and several SEM pictures taken from different angles. Electrical characterization of the devices will take place shortly.

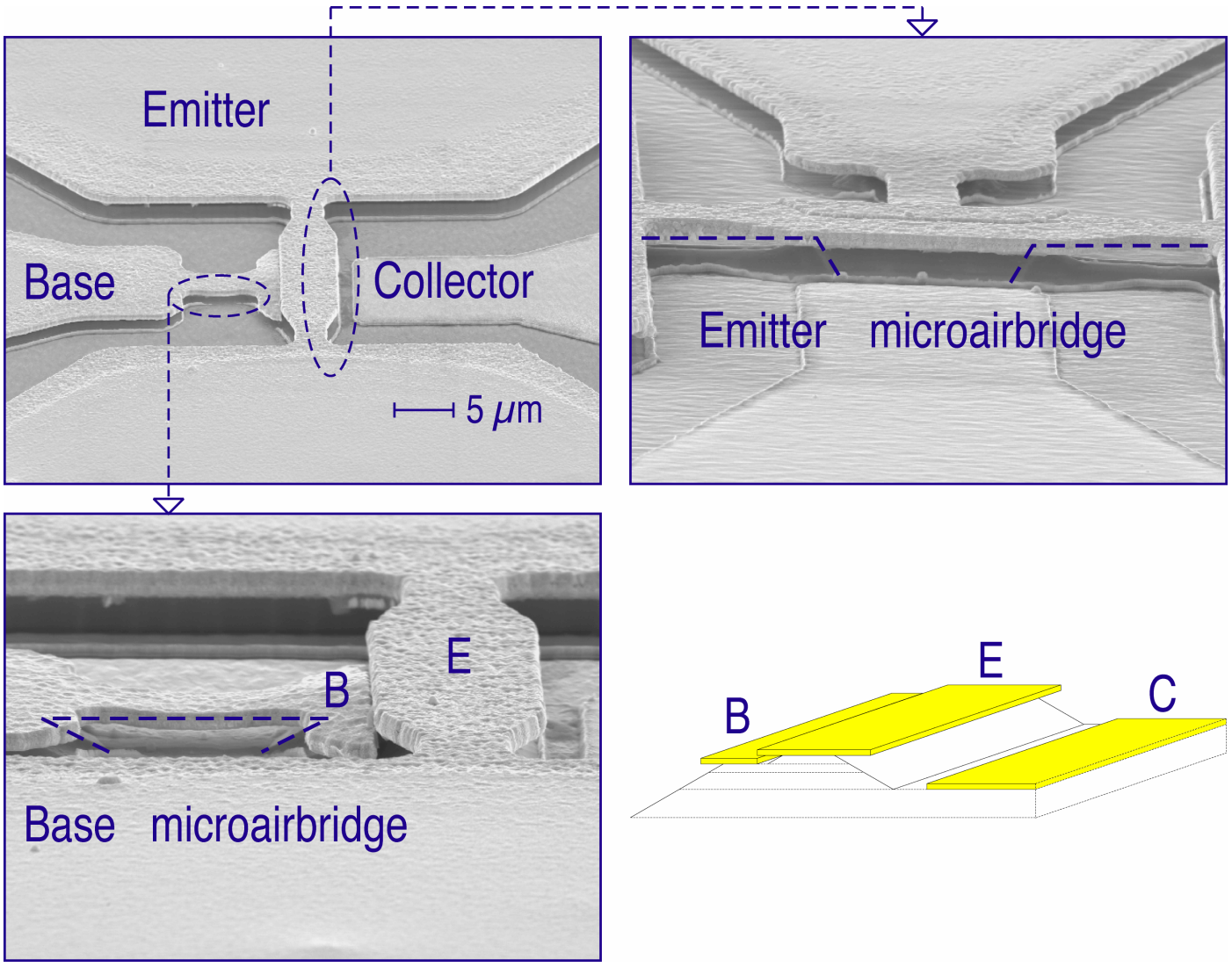

Figure 10. Schematic and SEM pictures of a HBT device using airbridges for electrode isolation.

An on-chip frequency-domain submillimeter-wave spectrometer

Sponsor
Rosenblith Fellowship

Project Staff
Juan Montoya and Q. Hu

Because of the frequency limitation of semiconductor electronic devices, measurement instruments such as network analyzers can operate only below approximately 100 GHz. Thus, even if ultrahigh-frequency HBTs can be developed, they can only be directly measured up to 100 GHz, with higher-frequency performance extrapolated according to certain frequency roll-off models. Clearly, such an extrapolated measurement will not be applicable to measuring high-frequency resonance such as that shown in Fig. 9. It will be very useful to develop on-chip systems that can characterize device performance up to THz frequencies. A promising component for such systems is ultrafast photoconductive switches made of low-temperature-grown (LTG) GaAs materials. When pumped with two coherent laser beams, such switches can generate and detect photocurrent with a modulation frequency beyond one THz.

Furthermore, photoconductive emitters and receivers are attractive as components of sub-millimeter-wave spectroscopy systems because of their tunability, compactness and ability to be monolithically integrated with antennas, transmission lines and microelectronic devices. Such systems can be classified either as time-domain or frequency-domain systems. Time-domain systems, which contain a photoconductive pulse emitter and sampler excited by a mode-locked laser, are the most investigated. They have been used for free-space characterization of semiconductor materials, and on-chip characterization of ultrafast devices and circuits with 2.7 ps time resolution. The frequency resolution is the inverse of the time span over which the propagating pulse is sampled. This span is determined by the length of an optical delay line, which usually results in a frequency resolution broader than 1 GHz.

The emitter and receiver of a frequency-domain spectrometer will be pumped by two coherent cw laser beams with frequencies ω_1 and ω_2, instead of short laser pulses. If the response time is sufficiently fast, the emitter switch will generate an ac photocurrent with a frequency $|\omega_2-\omega_1|$, which can easily exceed 1 THz. Illuminated by the same two laser beams with a controlled delay, the receiver switch can be used to perform a homodyne detection of the ac photocurrent generated from the emitter. In combination with high-frequency transmission lines, they can form on-chip spectrometers with THz bandwidths. Fig. 11 illustrates a schematic of such a spectrometer that can be used to characterize common-emitter performance of high-frequency HBTs.

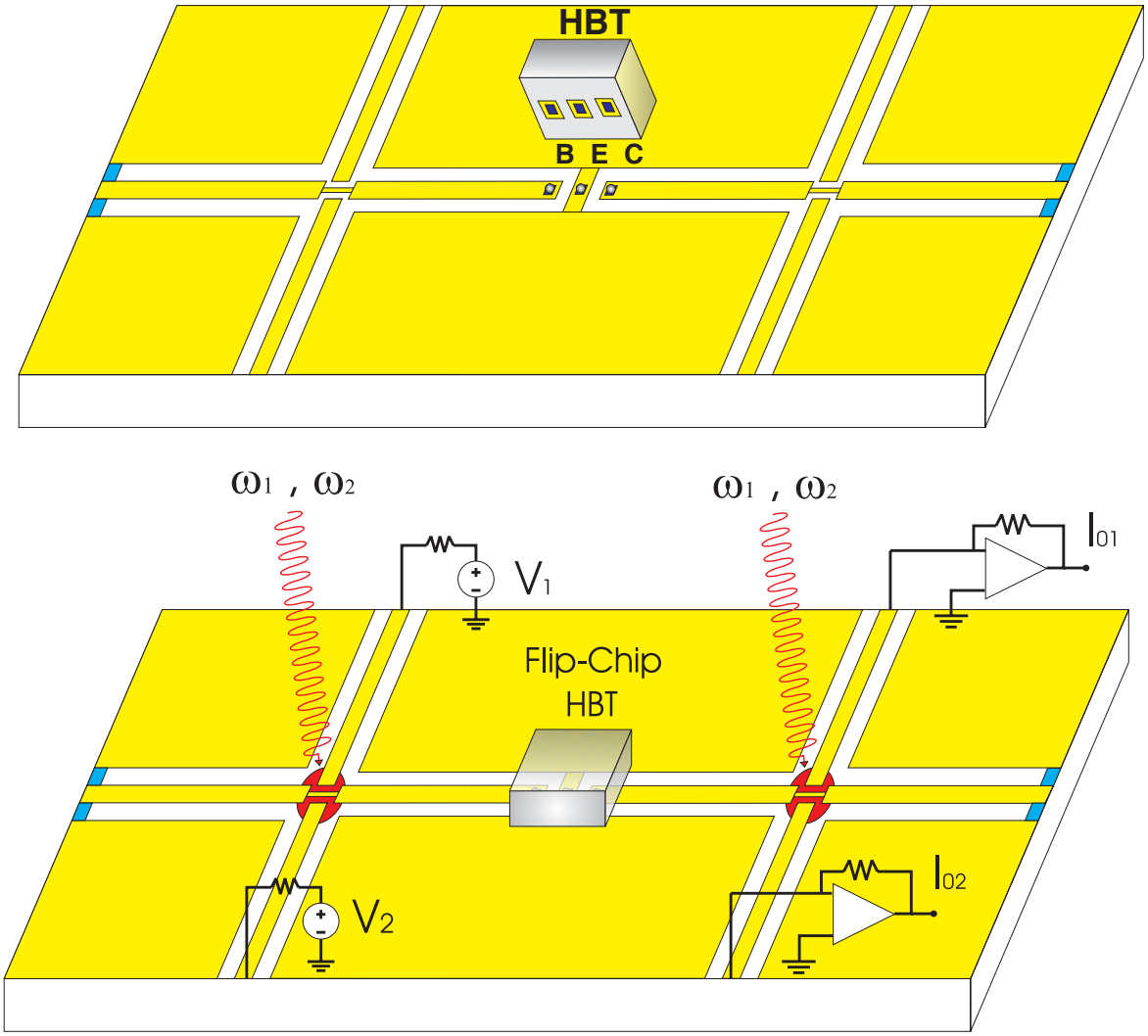

Figure 11. Schematic of a on-chip spectrometer that uses ultrafast photoconductive switches to generate and detect ultrahigh-frequency signals.

Because of the broad bandwidth (>1 THz) and a high frequency resolution (better than 1 MHz), such a spectrometer is also adequate for molecular line spectroscopy. In combination with microchambers, the spectrometer can be part of a microfluidic, "lab on a chip"-type circuit, which can be used as on-chip sensors for chemical and biological agents. As the first step in the development of an on-chip frequency-domain spectrometer, we have investigated the performance of an on-chip transceiver containing only uninterrupted coplanar waveguides (CPWs).

In order to improve the coupling efficiency of the photoconductive switches and to reduce their RC time constants, we used interdigited finger electrodes fabricated using e-beam lithography. A schematic and a SEM picture of such a photoconductive switch are shown in Fig. 12.

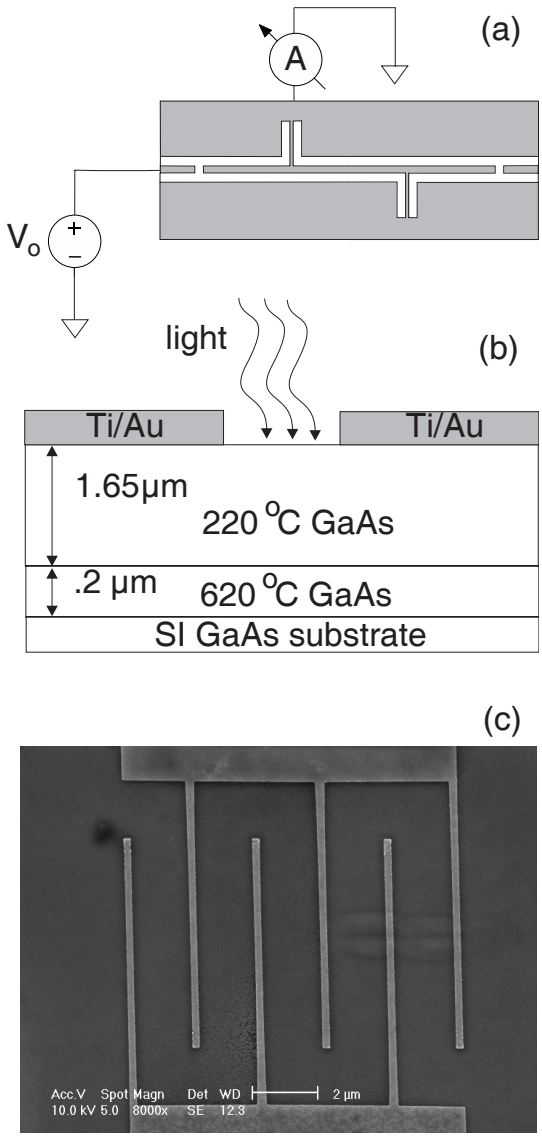

Figure 12. Schematic and SEM picture of a photoconductive switch with interdigited finger geometry and fabricated using e-beam lithography.

Previously, we have shown that LTG-GaAs photoconductive switches embedded in a transmission line can function as an intensity-intensity autocorrelator, based on the nonlinearity of a voltage divider including the photoconductive switch and the characteristic impedance of the transmission line. The time resolution of this autocorrelator, however, is limited by the response time of the LTG-GaAs photoconductive switch, which is on the order of 1 ps. In order to improve the time resolution of the autocorrelator to the degree that it can resolve the time span of femtosecond laser pulses, a more intrinsic nonlinear process must be used than the voltage divider scheme. In a recent experiment, we have developed a much faster autocorrelator by using two-photon absorption process in the photoconductive switch. The almost instantaneous nature of this nonlinear process greatly improves the time resolution of the autocorrelators. Fig. 13 shows the measured time profile of fs laser pulses from a mode-locked Ti:sapphire at 900-nm wavelength. At this long wavelength, the photon energy is smaller than the energy gap of LTG-

GaAs, thus single photon absorption is suppressed. As can be seen from Fig. 13, the pulse shape measured using this novel autocorrelator is in good agreement with that measured using a conventional autocorrelator with SHG crystals. This development could lead to compact, alignment free autocorrelators with femtosecond time resolutions. Furthermore, the gap energy of LTG-GaAs will make it a natural candidate for the two photon absorption measurements at ~1500-nm wavelength, which is important for fiber telecommunications.

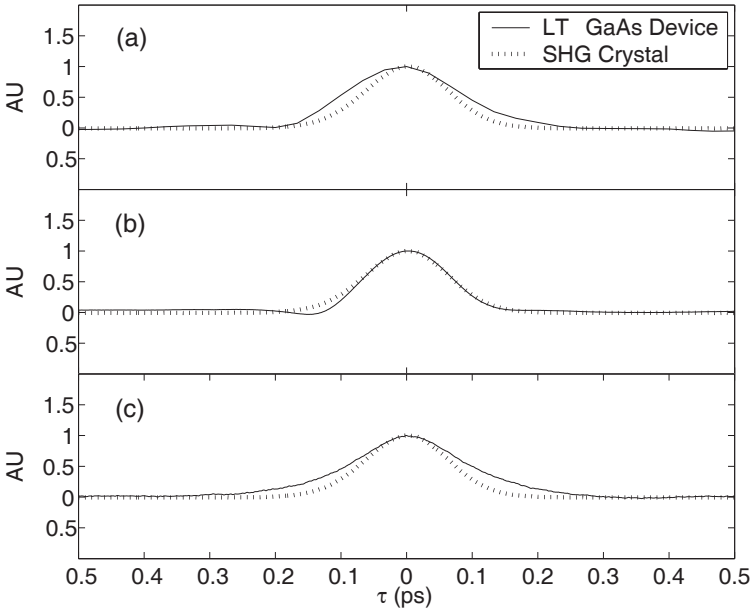

Figure 13. Two photon absorption autocorrelation at 900-nm wavelength with an average laser power of 170 mW.

Patent applications, Publications, and Conference Presentations

1. Qing Hu and Benjamin S. Williams, "Metal Waveguides for Mode Confinement in Terahertz Lasers and Amplifiers," M.I.T. Case No. 10279 (2003).

2. Qing Hu and Benjamin S. Williams, "Terahertz Lasers and Amplifiers Based on Resonant Optical Phonon Scattering to Achieve Population Inversion," M.I.T. Case No. 10280 (2003).

3. B. S. Williams, H. Callebaut, S. Kumar, Q. Hu, and J. L. Reno, "3.4-THz quantum cascade laser based on LO-phonon scattering for depopulation," Appl. Phys, Lett. **82**, 1015 (2003). Also published in Virtual Journal of Nanoscale Science & Technology, **7**(8), (2003).

4. B. S. Williams, S. Kumar, H. Callebaut, Q. Hu, and J. L. Reno, "3.4 THz quantum cascade laser operating above liquid nitrogen temperature," Electro. Lett. **39**, 915 (2003).

5. H. Callebaut, S. Kumar, B. S. Williams, and J. L. Reno, "Analysis of transport and thermal properties of THz quantum cascade lasers," Appl. Phys. Lett. **83**, 207 (2003).

6. J. Montoya and Q. Hu, "LT-GaAs Coplanar Waveguide Single Photon/Two Photon Absorption Autocorrelator," J. Appl. Phys. **95**, 2230 (2004). Also published in Virtual Journal of Ultrafast Science, March (2004).

7. B. S. Williams, S. Kumar, H. Callebaut, Q. Hu, and J. L. Reno, "Terahertz quantum cascade laser at $\lambda \approx 100$ μm using metal waveguide for mode confinement," Appl. Phys. Lett. **83**, 2124 (2003).

8. Q. Hu, B. S. Williams, S. Kumar, H. Callebaut, and J. L. Reno, "Terahertz quantum cascade lasers based on resonant phonon scattering for depopulation," Phil. Trans. R. Soc. London **A362**, 233-249 (2004).

9. B. S. Williams, S. Kumar, H. Callebaut, Q. Hu, and J. L. Reno, "Terahertz Quantum Cascade Lasers Operating up to 137 K," Appl. Phys. Lett. **83**, 5142 (2003).

10. H. Callebaut, S. Kumar, B. S. Williams, Q. Hu, and J. L. Reno, "Importance of electron-impurity scattering for electron transport in THz quantum-cascade lasers," Appl. Phys. Lett. **84**, 645 (2004).

11. S. Kumar, B. S. Williams, S. Kohen, Q. Hu, and J. L. Reno, "Continuous-wave operation of terahertz quantum-cascade lasers above liquid-nitrogen temperature," to be published in Appl. Phys. Lett. April (2004).

12. B. S. Williams, S. Kumar, Q. Hu, and J. L. Reno, "Resonant-phonon terahertz quantum-cascade laser operating at 2.1 THz ($\lambda \approx 141$ μm)," to be published in Elect. Lett. (2004).

13. B. S. Williams, "Development of THz quantum-cascade lasers", 33rd Winter Colloquium on The Physics of Quantum Electronics, Snowbird, Utah, January 7, (2003). (Invited)

14. M. N. Gurnee, L. D. Kimball, and Q. Hu, "Characterization of VOx as a High Performance Microbolometer Detector," presented at 2003 Meeting of the Military Sensing Symposia (MSS) Specialty Group on Detectors, Tucson, Arizona, February 24-28, (2003), published in the symposium proceedings.

15. Benjamin S. Williams, Hans Callebaut, Sushil Kumar, Qing Hu, and John L. Reno, "Terahertz quantum cascade laser based on direct LO-phonon-scattering depopulation," presented at the 2003 APS March meeting in session **X8.013**, Austin, TX, March (2003).

16. Q. Hu, Benjamin S. Williams, Hans Callebaut, Sushil Kumar, and John L. Reno, "Terahertz quantum cascade laser based on LO-phonon-scattering assisted depopulation," presented at SPIE Aerosense Symposium, Orlando, FL, April (2003). (Invited)

17. B. S. Williams, H. Callebaut, S. Kumar, Q. Hu, and J. L. Reno, "Terahertz quantum cascade laser based on LO-phonon-scattering assisted depopulation," CLEO/QELS 2003, Baltimore, Maryland, June 1-6 (2003).

18. Q. Hu, "Terahertz quantum cascade lasers based on resonant phonon scattering for depopulation," the Royal Society Scientific Discussion Meeting *The terahertz gap: the generation of far-infrared radiation and its applications*, London, UK, June 4-5 (2003). (Invited)

19. Q. Hu, "Terahertz Quantum Cascade Lasers Based on Resonant-Phonon-Scattering-Assisted Depopulation," presented at 2003 Advanced Research Workshop Future Trends in Microelectronics: *The Nano, the Giga, the Ultra, and the Bio*, Corsica, France, June 23-27, (2003). (Invited)

20. B. S. Williams, S. Kumar, H. Callebaut, Q. Hu, and J. L. Reno, "Terahertz Quantum Cascade Lasers Based On Resonant-Phonon Depopulation And Using Metal-Metal Waveguides," presented at the 5th International Conference on Intersubband Transitions in Quantum Wells (ITQW'03), Evolene, Switzerland, September (2003).

21. H. Callebaut, S. Kumar, B. S. Williams, Q. Hu, and J. L. Reno, "Analysis of transport properties of THz quantum cascade lasers," presented at the 5th International Conference on Intersubband Transitions in Quantum Wells (ITQW'03), Evolene, Switzerland, September (2003).

22. Q. Hu, "Terahertz Quantum Cascade Lasers," Chinese Physical Society Fall Meeting, Hefei, China, September 18-20, (2003). (Invited Plenary Talk)

23. Q. Hu, "THz quantum cascade lasers based on resonant phonon scattering for depopulation," The 11th IEEE International Conference on Terahertz Electronics (THz2003), Sendai, Japan, September 24-26, (2003). (Invited Plenary Talk)

24. Q. Hu, "THz quantum cascade lasers based on resonant phonon scattering for depopulation," The 28th International Conference on Infrared and Millimeter Waves (IRMMW2003), Otsu, Japan, September 29 – October 3, (2003). (Invited Plenary Talk)

25. Q. Hu, "THz quantum cascade lasers based on resonant phonon scattering for depopulation," The 16th Annual Meeting of the IEEE Lasers & Electro-Optics Society (IEEE/LEOS 2003), Tucson, AZ, October 26-30, (2003). (Invited)

26. Q. Hu, "Resonant-phonon-assisted THz quantum-cascade lasers using metal-metal waveguides for mode confinement," International Workshop on Quantum Cascade Lasers, Servile, Spain, January 4-7, (2004). (Invited)

27. B. S. Williams, S. Kumar, H. Callebaut, S. Kohen, Q. Hu, and J. L. Reno, "Terahertz quantum cascade lasers using resonant-phonon depopulation and metal-metal waveguides," IEEE Phonoics West, San Jose, CA, January 27 (2004). Published in SPIE Proceedings, vol. **xxx**, yyy (2004). (Invited)

28. Q. Hu, "Generation of Terahertz Emission Based on Intersubband Transitions," pp. 57-86, Advanced Semiconductor Heterostructures: Novel Devices, Potential Device Applications and Basic Properties, International Journal of High Speed Electronics and Systems, Vol. 12, No. 4, M. Dutta, and M. A. Stroscio, eds., World Scientific, Singapore, (2003).

29. Q. Hu, Benjamin S. Williams, Hans Callebaut, Sushil Kumar, and John L. Reno, "Terahertz quantum cascade laser based on LO-phonon-scattering assisted depopulation," presented at the 14th International Symposium on Space Terahertz Technology, Tucson, AZ, April (2003).

30. Hu, Q., "Terahertz Quantum-cascade Lasers," presented at the 2004 APS March meeting in session **Y2.004**, Montreal, Canada, March (2004). (Invited)

31. Hu, Q., "Terahertz Quantum-cascade Lasers," presented at the 2nd International Symposium on Ultrafast Phenomena and Terahertz Waves, Shanghai, China, May (2004). (Invited)

32. B. S. Williams, S. Kumar, Q. Hu, and J. L. Reno, "Resonant-phonon terahertz quantum cascade lasers at long wavelengths," session CMZ1, CLEO/QELS 2004, San Francisco, CA, May (2004).

33. S. Kumar, B. S. Williams, S. Kohen, Q. Hu, and J. L. Reno, "High temperature continuous-wave operation of terahertz quantum cascade lasers," session CMZ2, CLEO/QELS 2004, San Francisco, CA, May (2004).

34. Q. Hu, "Terahertz Quantum Cascade Lasers," presented at the 6th International Conference on Mid-infrared Optoelectronics Materials and Devices (MIOMD-VI), St. Petersburg, Russia, June (2004). (Invited)

Theses

Ph.D. thesis

Benjamin S. Williams, thesis title, "Terahertz quantum cascade lasers," August, 2003.